arXiv:1402.3504v1 [astro-ph.HE] 14 Feb 2014

Calculations of radio emission from ultra-high energy cosmic ray air showers: a practical approach.

Jaime Alvarez-Muñiz, [a] Washington R. Carvalho Jr., [a]
Harm Schoorlemmer, [b] Enrique Zas [a]

[a] *Departamento de Física de Partículas & Instituto Galego de Física de Altas Enerxías, Universidade de Santiago de Compostela, 15782 Santiago de Compostela, Spain*

[b] *University of Hawaii at Manoa, Department of Physics and Astronomy, Honolulu, Hawaii 96822, USA*

Abstract

A simple method has been devised to reduce the computing time needed to calculate the electric field of radio pulses emitted from air showers. It relies on an approximate description of the patterns of the radio pulses produced by two different mechanisms: the excess charge and the geomagnetic deviation of the charged particles. The amplitudes of the electric field due to each of these mechanisms must be calculated in Monte Carlo simulations but only at a few positions along a line at ground level. The amplitudes at other positions are deduced using the projected Cherenkov cone on the ground. The polarization patterns of the electric field due to each mechanism are different and are taken from relatively well known properties of the radio emission in air showers. The results of this approach, that can be obtained with modest computing resources, are shown to agree at a few percent level with full Monte Carlo simulations.

Key words: high energy cosmic rays, extensive air showers, Cherenkov radio emission
PACS: 95.85.Bh, 95.85.Ry, 29.40.-n,

1 Introduction

In the last few years there has been a flurry of activity to explore the potential of the radio technique to study ultra high energy cosmic rays (UHECRs) [1]. The technique is attractive because it requires detectors which are relatively cheap and is not limited by a small duty cycle, unlike the fluorescence

technique [2]. Several experimental initiatives such as AERA [3] and EASIER [4] in coincidence with the Pierre Auger Observatory [5], CODALEMA [6], LOPES [7], TREND [8], LOFAR [9] and Tunka-Rex [10], have been exploring emission from air showers mainly in the 30-80 MHz frequency range, studying the relation of the pulses to composition [11,12] and trying to understand the lateral distribution of the emission [13,14,3,9]. In addition the fortuitous detection of pulses from air showers with the ANITA balloon flown detector [15] has revealed that the pulses from these showers extend to the GHz regime, with more experimental evidence also obtained by the CROME experiment [16]. These studies are considered of primordial importance to explore the viability of the radio technique either to provide an alternative design of future air shower arrays covering areas in the range of 10,000 km^2 and above, or to use them as complementary detectors that could help to constrain the composition of the cosmic rays on a shower-by-shower basis.

On the phenomenological side there has also been a lot of progress. Calculations have been made based on the macroscopic treatment of the current densities that arise in these showers [17,18], and also on more detailed simulations that use the superposition principle to calculate the emission adding the contributions from single particle sub-tracks [19,20,21,22]. The results of these calculations, that reproduce pulses extending into the GHz regime as detected by ANITA [23], are now in reasonably good agreement [25] and they have been successfully tested against data [26,23,3,27,1]. As a result there is much more confidence in the calculations and it is believed that it is now possible to infer properties of the shower such as direction, energy and shower maximum using only measurements of the radio pulses in antennas scattered at ground level [28,29,30,31,1].

The study of the capabilities of these detectors as well as the reconstruction of cosmic ray shower parameters in detail requires full simulations of the shower and the radio pulses at a large variety of locations what becomes quite demanding of computing resources. This has become a natural obstacle for progress since these simulations have to be performed for a wide range of energies, shower geometries and primary particle compositions what inevitably is a very lengthy and arduous task. Needless to say that a comprehensive parameterization of the patterns of the electric field at ground level would be most welcome as an alternative. The approach presented here can be considered a step forward in this direction, since it can also simplify the creation of parameterizations.

In this work we have devised a phenomenological technique to reproduce the pattern of the radio pulses at ground level under most circumstances. The technique relies on standard approximate assumptions [17] and experimental observations of the characteristics of the radiation [32,33,6,27]. These are mainly due to two different radiation mechanisms, namely the excess negative

charge predicted by Askaryan in the 1960s, the Askaryan mechanism [34], and that induced by the interactions of the particles with the magnetic field of the Earth that induces a net current perpendicular to the shower axis, the geomagnetic mechanism [35]. We present here a method that exploits these general ideas and subsequently test the level of accuracy that it provides comparing the obtained results directly with the detailed simulations. The devised method reduces the calculation of the pattern at ground level to the pattern along a single line which can be sampled at a few points. This has a drastic effect on the required computing resources and has many applications for both the reconstruction of events at a given experimental facility or for design studies of future experimental arrangements.

This paper is organized as follows. In Section 2 we briefly review the main properties of radio emission in atmospheric cosmic ray showers. In Section 3 we describe a simple model to obtain the electric field induced by ultra-high energy cosmic ray showers in the atmosphere. The model only needs as input the separate amplitudes of the electric field induced by the geomagnetic and Askaryan contributions at a few positions on the ground, as obtained in Monte Carlo simulations. It then assumes a radial symmetry of the geomagnetic and Askaryan amplitudes and exploits the expected polarization of each mechanism to obtain the net electric field at any position on the ground. In Section 4 we compare the electric field calculated with this approach with that obtained in full Monte Carlo simulations. Finally, in Section 5 we conclude the paper and discuss future prospects.

2 Basics of radio emission in air showers

2.1 Radio emission mechanisms

Radio emission from showers initiated by cosmic rays in the atmosphere is discussed in terms of two mechanisms: the deflection of charges in the magnetic field of the Earth, the geomagnetic effect, and the development of an excess charge as the shower entrains electrons from the atmosphere into the shower front, the Askaryan mechanism. The different nature of the two mechanisms becomes apparent when we consider shower development without the magnetic field and only the Askaryan contribution exists.

The solution of Maxwell's equations in the transverse gauge relates the vector potential to the transverse current density, which in the limit of far observation distances is simply the projection of the current orthogonal to the direction of observation [36,37,39]. This is evident in a microscopic approach where currents are regarded as a sample of small particle sub-tracks of charge q moving

at constant velocity $\vec{v}$, each of them contributing in proportion to $q\vec{v}_\perp$ [38,39], where $v_\perp$ refers to the projection of the sub-track into a plane perpendicular to the observation direction. The fact that the index of refraction is not constant in the atmosphere, that the particle tracks are not perfectly parallel to the shower axis and that the observation direction changes for each particle track complicates the picture but does not alter this fact.

The two mechanisms can be related to different components of the current density, perpendicular and parallel to the shower axis. The perpendicular component of the current is related to the geomagnetic mechanism and results from the Lorentz force induced by the geomagnetic field $\vec{B}$ that accelerates the charges in the direction $q\vec{v}\times\vec{B}$ [1]. For the shower as a whole this current scales with $|\vec{B}|\sin\alpha$, with α the angle between $\vec{V}$ and $\vec{B}$, where $\vec{V}\simeq<\vec{v}>$ is assumed to be parallel to shower axis. So the magnitude of the vector potential, hence the electric field, depends strongly on both the zenith, θ, and azimuth, ϕ, angles of the shower, which determine the value of α. Since electrons and positrons deviate in opposite directions they both contribute with the same sign to this component. The polarization to be expected for the vector potential is simply given by the projection of the $-\vec{V}\times\vec{B}$ direction transverse to the observation direction. For observers positioned along the shower axis this coincides with $-\vec{V}\times\vec{B}$. This is the main mechanism for the radiation in extensive air showers.

The component of the current that is parallel to shower axis is related to the Askaryan mechanism and arises because of the excess electrons in the shower front. The magnitude of the vector potential from this contribution is directly related to the excess charge as the shower develops in the atmosphere and the arrival direction of the shower has little effect on the magnitude of this excess. The polarization of the vector potential is along the projection of the shower direction onto the plane transverse to the observation direction, and has radial symmetry. It is thus zero along the shower axis and increases in proportion to $\sin\beta$, where β is the angle between the shower axis and the observation direction [37,39]. The polarization of the vector potential has thus a strong radial component which increases as the observer deviates further away from shower axis.

2.2 Cherenkov like effects

The fact that the refractive index n of the atmosphere is greater than 1 is of utmost importance to understand the radio emission from air showers [40,18,21]. Since radio waves in air travel slightly slower than the shower particle front,

[1] This has been referred to as a *transverse* current in the sense that it lies in a plane perpendicular to the shower axis.

shock wave effects similar to those observed in Cherenkov radiation play an important role in the time dependence of the electric field as seen by an observer on ground [18,21]. This in turn determines the amplitude and frequency spectrum of the observed radiation. In a simplified one-dimensional shower model [23], the emission from the point in the shower development that is seen by a particular observer at the Cherenkov angle arrives first and, more importantly, the emission from a region around it arrives with a much smaller delay than the rest of the shower. This is the result of the relation between observation, t, and retarded, t^*, times which is such that t has an absolute minimum with $dt/dt^* = 0$ in the Cherenkov direction [40,21]. The vector potential has an abrupt growth at this minimum t due to an effective "time compression" of the contributions from a relatively large region of the shower. This induces a strong and narrow pulse, coherent up to frequencies in the $\sim$ GHz and with an enhanced power [15,16,23]. An observer thus becomes much more sensitive to the region of the shower seen at angles close to the Cherenkov angle. When the antenna lies in the Cherenkov direction with respect to the depth of maximum shower development, $X_{\rm max}$, the detected electric fields are the largest, since more particles contribute to either of the mechanisms. These points of maximum radiation define a circular ring-like region on the plane perpendicular to the shower axis, or equivalently an elliptical region when projected onto ground given by the intersection of a Cherenkov cone centered at $X_{\rm max}$ with ground level. The major (r_a) and minor (r_b) axis of the ellipse are approximately given by [2]:

$$
\begin{aligned}
r_a &= \left[\tan\left(\theta + \theta_{\rm Cher}\right) - \tan\theta\right] \; h_{X_{\rm max}} \\
r_b &= \frac{\tan\theta_{\rm Cher}}{\cos\theta} \; h_{X_{\rm max}}
\end{aligned}
\tag{1}
$$

where θ is the zenith angle of the shower, $h_{X_{\rm max}}$ is the height above ground of the position of shower maximum, and $\theta_{\rm Cher}$ is the Cherenkov angle at that height [3]. The major and minor axes of the Cherenkov ellipse on the ground scale with $h_{X_{\rm max}}$ and also increase as the angle θ rises.

[2] It is worth noting that the center of the ellipse is not exactly at the shower core. This is a small effect since the Cherenkov angle (opening angle of the cone) is typically smaller than 1°, we nevertheless use exact expressions in the approach described in Section 3.

[3] The refractive index decreases with atmospheric altitude and $\theta_{\rm Cher}$ follows the same behavior.

2.3 Radiation pattern at ground level

The electric fields induced by the Askaryan and geomagnetic mechanisms interfere with each other to produce the total field at the observer position [17,19,20,21]. Since the amplitude of the geomagnetic field is strongly dependent on shower arrival direction, while the Askaryan field is not, the relative contributions of these two mechanisms vary strongly with shower geometry. For some particular arrival directions, Askaryan emission can actually dominate the radio emission, e.g. when the shower axis is parallel to the direction of the magnetic field and $\alpha \simeq 0^\circ$. Some examples will be shown below. The region where the signal is largest is pretty much concentrated in a Cherenkov cone with vertex at shower maximum. This sets the scale of the radiation pattern at ground, given by r_a and r_b in Eq. (2). As the Cherenkov angle is very small, typically less than 1°, the direction of observation of the shower region where the contribution is largest is nearly parallel to the shower axis and this allows some approximate simplifications. Taking the direction of observation parallel to the shower direction, the Askaryan polarization, $\hat{a}$, is radial with respect to the shower axis while the geomagnetic polarization, $\hat{g}$, has a constant direction given by $-\vec{V} \times \vec{B}$ (see Fig. 1). The different patterns of the polarization vector for the two mechanisms create asymmetries in the footprint of the radio signal on the ground that, depending on the geometry of the shower and the observer position, can be very sizeable [17,19,20,21]. The full description of the radio emission pattern at ground level requires a two dimensional function.

3 A simple model

Here we describe a simple model that makes use of approximate symmetries which are only present when the two dominant emission mechanisms are considered separately. Using as input the separate geomagnetic and Askaryan contributions to the electric field at only a few simulated antenna positions, we are able to predict with great accuracy the total electric field at any position on the ground. We only assume that the amplitudes of both contributions depend only on the radial distance to the shower axis and exploit the approximate polarization patterns described in the previous section for both mechanisms. This considerably reduces the CPU time needed to obtain an accurate description of the two-dimensional pattern of the electric field on ground which will be described in terms of r, the distance to shower core, and ϕ, the polar angle of the vector from the impact point of the shower to the observer.

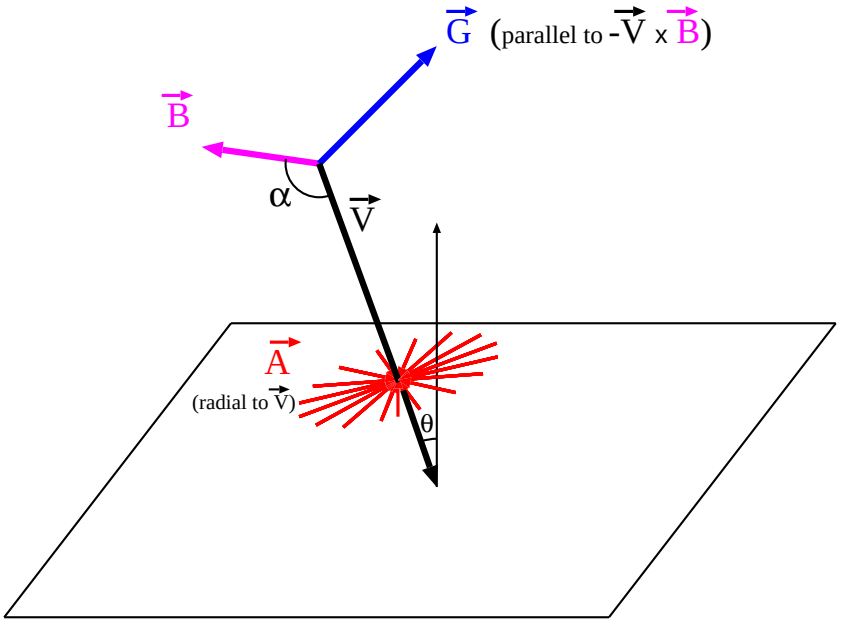

Fig. 1. Scheme of the axis of a shower along with the polarization of the emission due to the geomagnetic ($\vec{G}$) and Askaryan ($\vec{A}$) mechanisms. $\vec{B}$ is the geomagnetic field pointing North and $\vec{V}$ marks the direction of shower axis. The amplitudes of the geomagnetic and Askaryan fields drawn in the sketch are for illustrative purposes only and not to scale.

3.1 Assumptions

Our approach is based on a few assumptions regarding the radio emission. Some stem from well-known features of the electric field induced by the geomagnetic and Askaryan mechanisms:

(A) The polarizations of the electric field induced by the geomagnetic ($\hat{g}$) and Askaryan ($\hat{a}$) emission mechanisms are linear and follow the expected theoretical predictions (see Section 2.3 and Fig. 1):

$$\hat{g} = \frac{-\vec{V} \times \vec{B}}{|-\vec{V} \times \vec{B}|} \quad \text{and} \quad \hat{a} = \hat{r} \tag{2}$$

with $\hat{r}$ a radial unit vector that points from the antenna position to the shower axis and is perpendicular to it, i.e. $\hat{r}$ is on the transverse shower plane (perpendicular to the shower direction) that contains the antenna position.

(B) The amplitude of the electric field induced by each emission mechanism separately is circularly symmetric in the transverse plane of the shower, i.e. it depends only on distance to the shower axis. Equivalently, the amplitude of the field on the ground for each mechanism is constant along ellipses similar to the elliptical Cherenkov ring (see Section 2.2 and

Fig. 2).

(C) Both $\vec{E}_{\rm geo}(t)$ and $\vec{E}_{\rm Ask}(t)$ are accessible through Monte Carlo simulations of air shower development and associated radio emission such as those performed with the ZHAireS code described in [21].

(C.1) $|\vec{E}_{\rm Ask}|(t)$ at any observer position, can be obtained in a shower simulation where the magnetic field of the Earth is artificially switched off. In that case the Askaryan mechanism is the only one contributing significantly to the total electric field. The assumption is:

$$\vec{E}_{\rm Ask}(t) = \vec{E}_{B_{\rm off}}(t) \tag{3}$$

(C.2) The electric field induced by the geomagnetic mechanism can be approximately obtained by subtracting the electric field as given in a simulation performed with the geomagnetic field switched on $\vec{E}_{B_{\rm on}}(t)$, from that obtained in the simulation with the magnetic field switched off described in the previous item [4]. For a particular observer position at time t:

$$\vec{E}_{\rm geo}(t) = \vec{E}_{B_{\rm on}}(t) - \vec{E}_{B_{\rm off}}(t) \tag{4}$$

3.2 Input and output observables

Our simple approach has been designed to predict a time independent vector observable $\vec{\mathcal{E}}$ related to the electric field and parallel to it by using as input only the amplitude of the same observable at a few observer positions. Several observables can be constructed from the full bandwidth pulse $\vec{E}(t)$ and different observables are used in each experiment to describe the electric field at ground level. Typically these observable definitions take into account detector characteristics such as its working frequency band. The model is independent of the actual precise definition of the chosen observable and the only restriction on the observable is that it should be a time independent measure of the electric field. Example choices are the average or the maximum of the electric field amplitude of the bandpass filtered pulse.

The only inputs in our approach are the amplitudes of the observable for each emission mechanism separately at a few observer positions on ground. The polarization is part of the model. These positions are chosen so that they lie at different distances R_i with respect to the shower core along a single direction, which hereafter will be referred to as the *reference line*. The input amplitudes for antennas along the chosen reference line are extracted from

[4] This procedure is in essence approximate since it is not possible to obtain exactly the same shower from simulations with and without the magnetic field. By using the same random seed in both simulations we can only obtain similar showers.

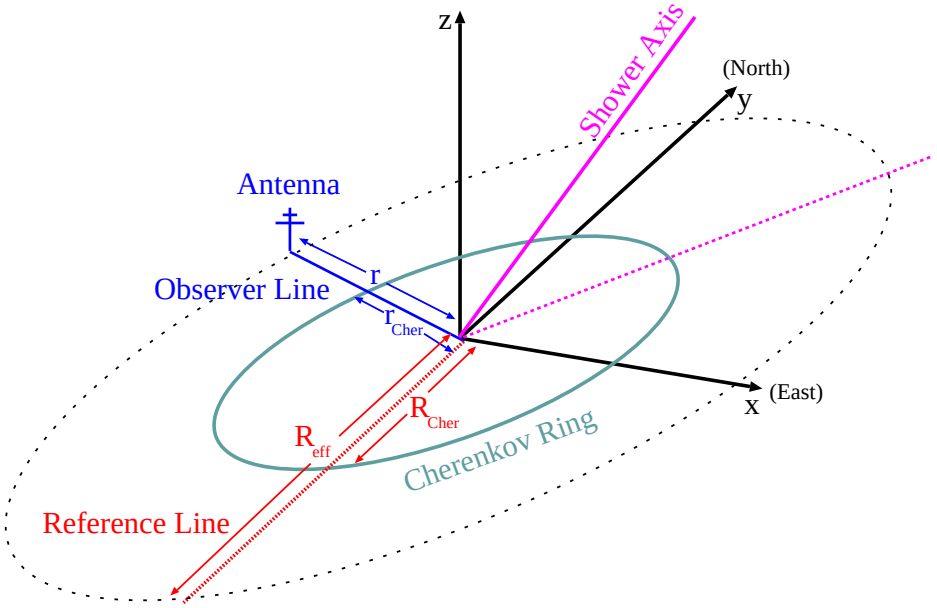

Fig. 2. Sketch of the geometry of the shower-observer system used in this work. We show the shower axis hitting ground (xy plane), the Cherenkov ellipse on ground where the peak electric field tends to be maximum and two lines: the "reference line" (in red, with distances to the core denoted as R), where the simulated electric field is used as input, and the "observer line" (in blue, with distances to the core denoted as r) where we apply the model to predict the electric field. We also show the distance to the Cherenkov ellipse along the reference line (denoted as $R_{\rm Cher}$) and along the observer line where the field is to be obtained (denoted as $r_{\rm Cher}$).

the full Monte Carlo simulations (see assumption C in Section 3.1). As will be shown later in this work, the actual direction chosen for the reference line is practically irrelevant, and we obtain accurate predictions for any reference line used as input. A sketch of the shower-observer geometry is shown in Fig. 2 where an example reference line is also depicted.

The actual observable used throughout this work is described in the following. For each antenna position R_i along the reference line, we first apply a band pass filter between 30 and 80 MHz to the simulated full bandwidth pulses $\vec{E}_{\rm geo}(R_i, t)$ and $\vec{E}_{i\,\rm Ask}(R, t)$ [5]. We use the amplitude of the analytical signal, which is obtained by a Hilbert transform of the filtered pulses and calculate the time dependent amplitudes for the geomagnetic, $|\vec{\mathcal{H}}_G|(R_i, t)$, and the Askaryan, $|\vec{\mathcal{H}}_A|(R_i, t)$, components. To obtain time independent quantities we finally take the maxima of these amplitudes at the selected points along the reference line,

[5] This bandwidth is currently being exploited in air shower radio detection experiments such as AERA [3], LOFAR [9] and CODALEMA [6].

$\mathcal{E}_G(R_i) = \max(|\vec{\mathcal{H}}_G|(R_i,t))$ and $\mathcal{E}_A(R_i) = \max(|\vec{\mathcal{H}}_A|(R_i,t))$. In the following we will loosely use $\vec{E}$ to denote the output observable as it is in fact an estimate of the electric field.

3.3 Methodology

It is straightforward to extrapolate the amplitudes $\mathcal{E}_G(R_i)$ and $\mathcal{E}_A(R_i)$ to any observer position (r,ϕ) and to obtain their expected polarizations following the assumptions described in 3.1.A. By adding these two contributions we can obtain the net electric field $\vec{E}(r,\phi)$, where r and ϕ are cylindrical coordinates in the ground plane.

Firstly, from the actual depth of maximum shower development $X_{\max}$ obtained in the simulation, we define the elliptical Cherenkov ring on the ground as given in Eq. (2). To obtain the amplitude of a given contribution at a given antenna position (r,ϕ) we draw a line joining it to the impact point of the shower axis, which we can refer to as the "observer line". As the amplitudes are assumed constant along ellipses similar to the Cherenkov ring the following relation applies [6]:

$$\frac{R_{\rm eff}(r,\phi)}{R_{\rm Cher}} \;=\; \frac{r}{r_{\rm Cher}(r,\phi)} \tag{5}$$

From the symmetry properties of the amplitude for each mechanism assumed in Section 3.1.B. above we obtain: $\mathcal{E}_G(r) = \mathcal{E}_G(R_{\rm eff})$ and $\mathcal{E}_A(r) = \mathcal{E}_A(R_{\rm eff})$.

Secondly, the expected polarization of the geomagnetic ($\hat{g}$) and Askaryan ($\hat{a}$) fields which depend on the direction of the shower axis ($\theta,\ \varphi$) and on the position of the observer, are obtained with the aid of Eq. (2). The resulting field is then given by [7]:

$$\vec{E}(r,\phi) = \mathcal{E}_G(R_{\rm eff})\ \hat{g} + \mathcal{E}_A(R_{\rm eff})\ \hat{a} \tag{6}$$

This expression applies regardless of the choice of observable as long as it represents a measurement of the electric field vector (see Section 3.2).

[6] The choice of the positions of the elliptical Cherenkov ring along the reference and observer lines in Eq. (5), although natural is somewhat arbitrary due to the assumed elliptical symmetry of the amplitudes on the ground.

[7] We use a simple linear interpolation to obtain the amplitudes at any given $R_{\rm eff}$ from the few antenna positions R_i used as input.

4 Results

Here we compare the predictions obtained using the methods described in this work with the results of full simulations of the radio emission performed with the ZHAireS code [21]. We demonstrate the validity of the assumptions of our model, as well as explore its range of applicability.

4.1 Monte Carlo simulations with ZHAireS

Using the ZHAireS code [21], we have produced sets of shower simulations with the parameters of the Pierre Auger Observatory site (LOFAR site) namely: ground altitude 1400 m (10 m) above sea level, and geomagnetic field of intensity 23 μT (49.25 μT) and inclination $-37°$ (67.8°).

The sets of simulations contain proton-induced showers at $E = 10^{17}$ eV arriving from the North $\varphi = 90°$ for both Auger and LOFAR sites, and from the West $\varphi = 180°$ (the South $\varphi = 270°$) for the Auger (LOFAR) site. For each azimuthal angle we have simulated showers with several zenith angles ranging from $\theta = 0°$ to $\theta = 80°$ in steps of $\Delta\theta = 5°$. We placed several observers at different distances from the shower core along 8 directions on ground, namely towards magnetic North (N), South (S), East (E), West (W), North East (NE), North West (NW), South East (SE) and South West (SW). Each shower geometry was simulated twice using the same random seed: once with the magnetic field switched on and once with it artificially switched off. The electric field induced by the geomagnetic and Askaryan mechanisms was obtained (as explained in Section 3) for each observer position and for each shower geometry.

For each shower geometry, a subset of the simulated pulses i.e. those at the positions that lie along a reference line, were used to construct the input of the model (see Section 3). These are used to predict the electric field at any other position away from the reference line, and in particular at the same positions where the pulses were simulated so that the comparison between the net field inferred from our method and that from the full simulation could be done. We calculated the same observable described in section 3.2 from the pulses obtained from full simulations.

As a first example we show in Fig. 3 the two-dimensional pattern of the electric field on the ground for a $\theta = 45°$ shower arriving from magnetic North at the LOFAR site. The amplitudes of the electric field at the antenna positions East of the core are used as input, and the electric field is obtained with the model at all other positions ($\sim 2 \times 10^5$ in total). The East-West asymmetry as well as the Cherenkov ring can be seen.

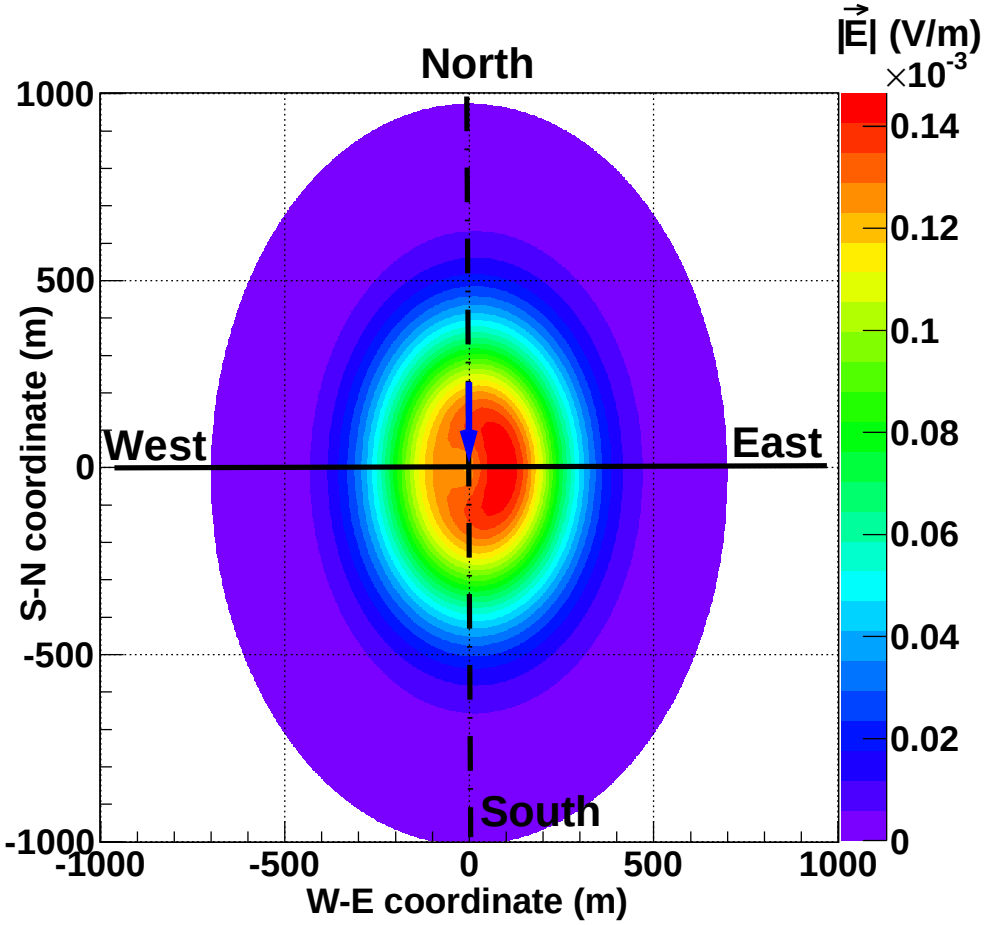

Fig. 3. Two-dimensional pattern of the amplitude of the electric field on the ground predicted by the simple model for a 10^{17} eV, $\theta = 45°$ shower arriving from magnetic North at the LOFAR site. We used 36 antenna positions as input to our approach, which are then used to estimate the signal in antennas at every 2 m in a rectangular grid (a total of $\sim 2 \times 10^5$ antennas).

4.2 Predictions compared to full simulation

With the aid of the simulations described before we tested the validity of our method to predict the total electric field at positions away from the reference line used as input.

We found a very good agreement between the predictions of the simple model and the Monte Carlo simulations in the vast majority of shower geometries. As an example, using the same configuration as in Fig. 3, we compare in Fig. 4 the components of electric field as obtained in the model with those in full simulations. In this particular example we used the line of antennas East of the core as the input reference line. The agreement is within a few percent for all distances to the shower core r and all directions. The shower geometry used in Fig. 4 results in the angle α between $\vec{V}$ and $\vec{B}$ of $\sim 112.8°$ or equivalently

$\sin\alpha \sim 0.92$. As a consequence the geomagnetic contribution dominates and the total electric field is dominated by the EW component (red lines), which is the direction of $-\vec{V} \times \vec{B}$ in this geometry.

The positions where the field reaches a maximum follow the expected elliptical shape of the Cherenkov ring. As expected for a shower coming from North, the major axis of the elliptical Cherenkov ring lies along the NS direction, while the minor axis lies along the EW direction. Also visible in Fig. 4 is the expected EW asymmetry in the value of the EW component of the field, which arises from the interference of the geomagnetic and Askaryan contributions. In the case of antennas that lie in the W-E line (top right panel of Fig. 4), the geomagnetic and Askaryan polarizations are both approximately parallel to the W-E line and point in the same direction for observers East of the shower core, and in the opposite direction for observers West of the core, leading to the asymmetry.

We have extensively tested our method for all the simulated showers. Some of these comparisons are summarized in Fig. 5, where we show the opening angle between the polarizations of the electric field predicted by the model and that obtained in the full simulation. The opening angle is shown as a function of shower zenith angle θ for observer positions along the West direction on the ground at several distances to the shower core. For each θ these distances are given relative to the distance $r_{\rm Cher}$ to the Cherenkov ring, e.g. $0.5\, r_{\rm Cher}$ (red squares) refer to positions half way between the core and the Cherenkov ring. It is important to notice that $r_{\rm Cher}$ increases with θ, and in this plot equal values of $r/r_{\rm Cher}$ for different θ correspond to different actual distances on the ground r. As can be seen in the figure, for showers with $\theta \gtrsim 20^\circ$ the opening angle is very small, below $\sim 2^\circ$. In the bottom panel of Fig. 5 we show the relative difference between the amplitude of the total electric field as obtained with our method and that from the full simulation for the same observers and shower geometries as in the top panel. The differences are smaller than $\sim 5\%$ for $\theta \gtrsim 20^\circ$. These comparisons demonstrate that the method works to a very good level of accuracy, validating the assumptions we made in Section 3. The more vertical showers with $\theta \lesssim 20^\circ$ will be discussed in Section 4.3.

In Fig. 6 we show a comparison between $|\vec{E}|$ as predicted by the model and as obtained in Monte Carlo simulations for showers at different zenith angles and along two directions on the ground, namely the EW (top) and NS (bottom) directions. Again, the agreement between our method and the simulations is at a few percent level. The Cherenkov ellipse is apparent, the major axis of the ellipse lying along the NS direction as expected for a shower coming from the North. The major and minor axes of the ellipse grow with increasing θ, mainly due to geometrical projection effects associated to the fact that the shower develops further from ground as θ increases. This is only partially compensated by a decrease of the Cherenkov angle because shower maximum occurs in a

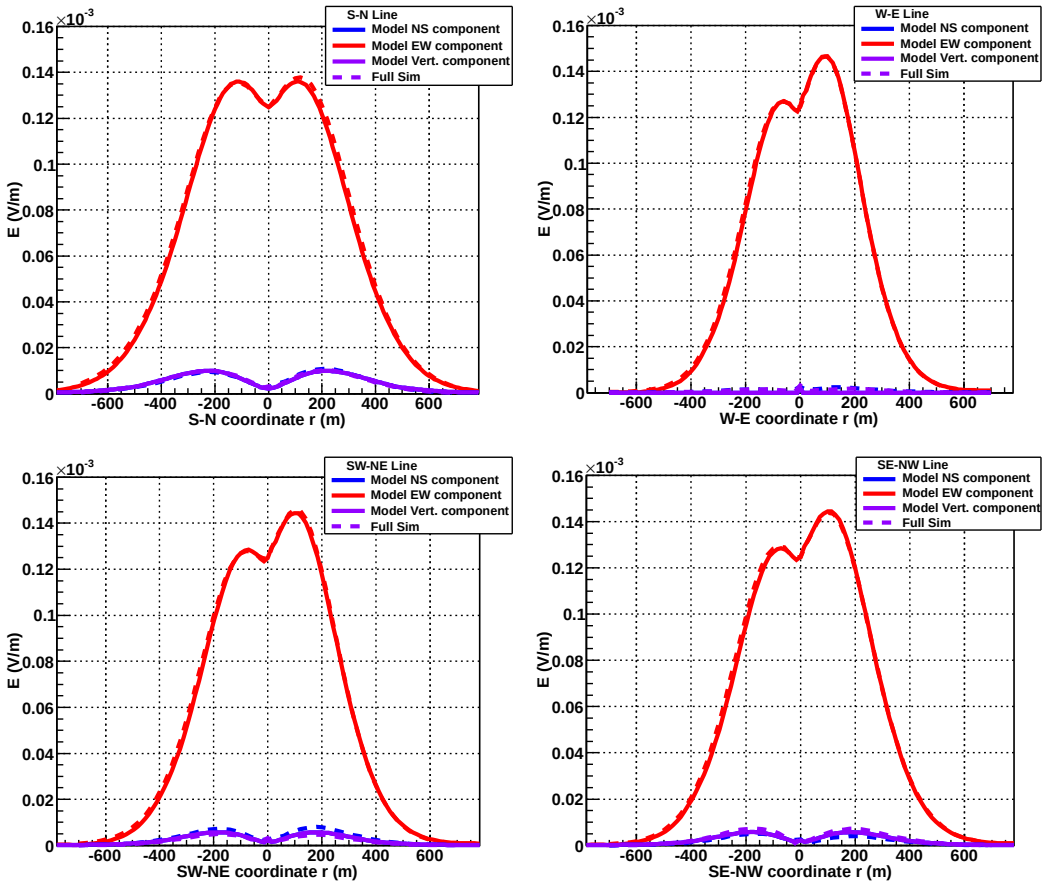

Fig. 4. Comparison of the components of the electric field as predicted by the model (solid lines) with those obtained in ZHAireS simulations (dashed lines) as a function of distance to the core r for observer positions along several directions on ground: South to North (top left), West to East (top right), South West to North East (bottom left) and South East to North West (bottom right). The geometry corresponds to a proton-induced shower of energy $E = 10^{17}$ eV coming from the North at $\theta = 45°$ at the LOFAR site. We used as input the amplitude of the electric field from the simulations at positions along the East direction (the reference line) and predicted the field components along all other lines shown in the plot. Negative values of r refer to S, W, SE and SW directions.

less dense atmosphere as the zenith angle increases [23]. In the most vertical shower shown in Fig. 6 the Cherenkov ellipse is less apparent, mainly because in less inclined showers the lateral extent of the shower becomes important [24]. As explained above, the asymmetry of the field along the EW direction is clearly visible in the top panel of Fig. 6. In the bottom panel of Fig. 6 one can see that the amplitude of the electric field North of the core is slightly underestimated. In this geometry ($\varphi = 90°$), antennas North of the core are closer to the shower than antennas South of the core, leading to larger fields North of the core. This early/late asymmetry is not yet included in the simple model.

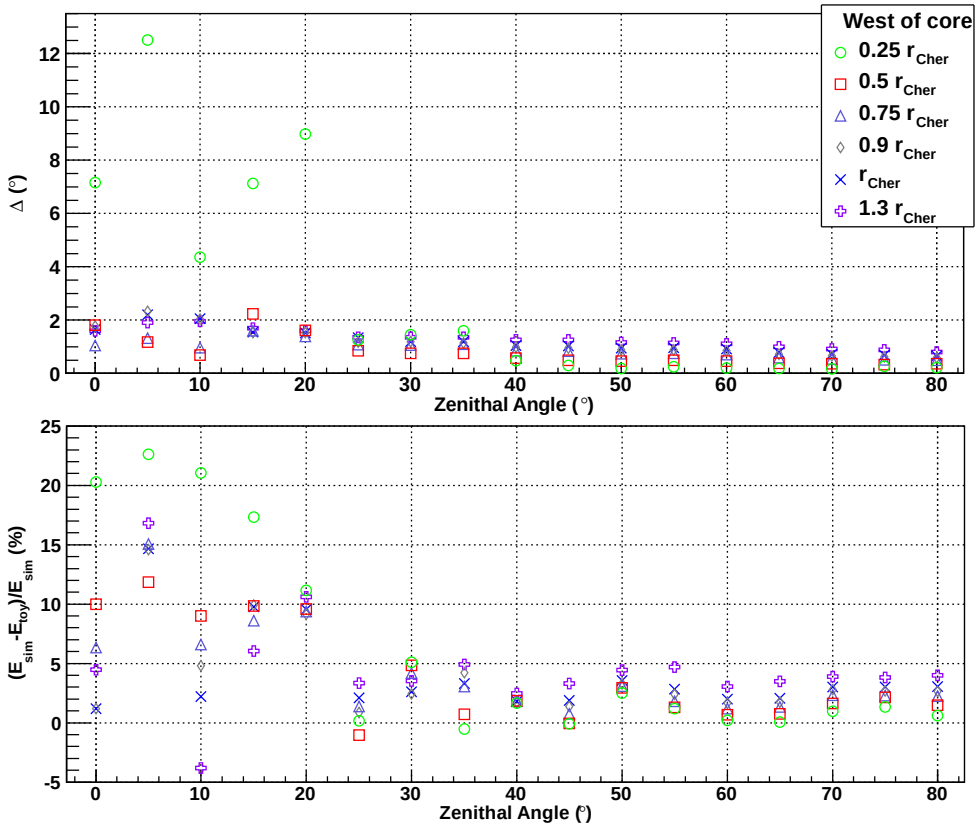

Fig. 5. Top: opening angle Δ between the total electric field predicted by the simple model and that obtained in the full simulation. The opening angle is shown as a function of shower zenith angle θ for several distances from the core and for observer positions along the West direction on the ground. The distances to the shower core are scaled to the distance to the Cherenkov ring $r_{\rm Cher}$ at each θ. The results correspond to proton-induced showers of energy $E = 10^{17}$ eV coming from the North at the LOFAR site. Observer positions along the East direction, not shown in the plot, were used as input. Bottom: relative difference between the amplitude of the net electric field as obtained with our method and that from the full simulation for the same observers and shower geometries as in the top panel.

As stated earlier in this work, the choice of the reference line, where the geomagnetic and Askaryan electric fields are simulated and used as input to the model, is mostly irrelevant. This is demonstrated in Fig. 7, where we show $|\vec{E}|$ as a function of distance to core along the W-E line for the same shower geometry as in Fig. 4. Each line in Fig. 7 represents the electric field obtained from the simple model using as input one of 4 different reference lines (see legend). One can see that there is only a small dependence on the choice of the reference line, which is mostly visible in the right hand peak around $r \simeq 100$ m. The main differences arise between the fields obtained when using as input the N and the S reference lines, and are understood in terms of early/late shower effects. Since the shower comes from the North, observers North of the core are closer to the shower than those at the South, inducing

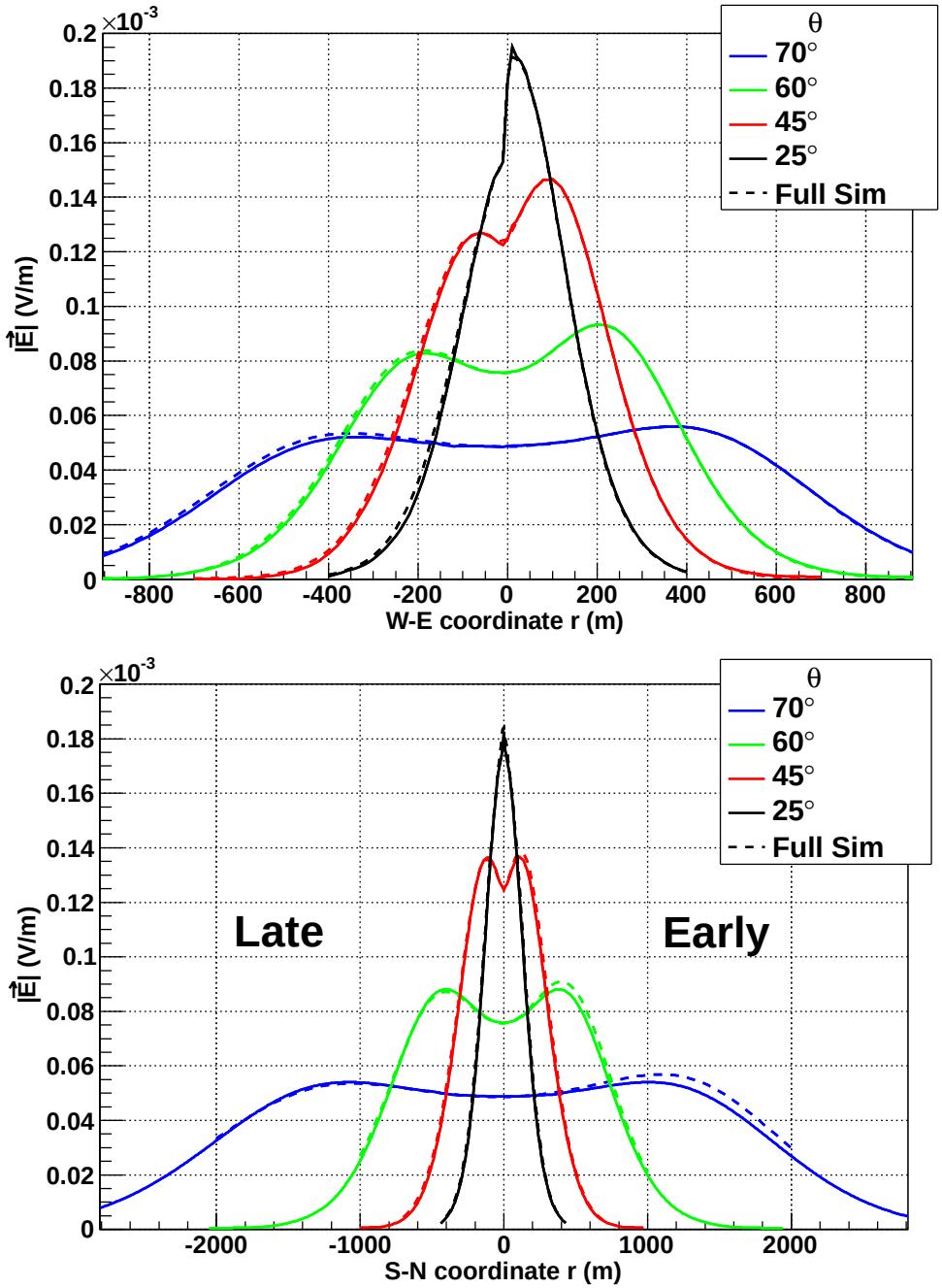

Fig. 6. Comparison of the modulus of the electric field $|\vec{E}|$ as predicted by the simple model (solid lines) with that obtained in ZHAireS simulations (dashed lines) as a function of distance to the core r for observer positions along the West to East (top) and South to North (bottom) directions on ground. The geometry corresponds to proton-induced showers of energy $E = 10^{17}$ eV coming from the North at different θ (see legend) at the LOFAR site. We used the amplitude of the electric field from the simulations on the positions along the East direction as inputs (the reference line) and predicted the field components along all other lines shown in the plot. Negative values of r refer to W (in the top panel) and S (bottom) directions.

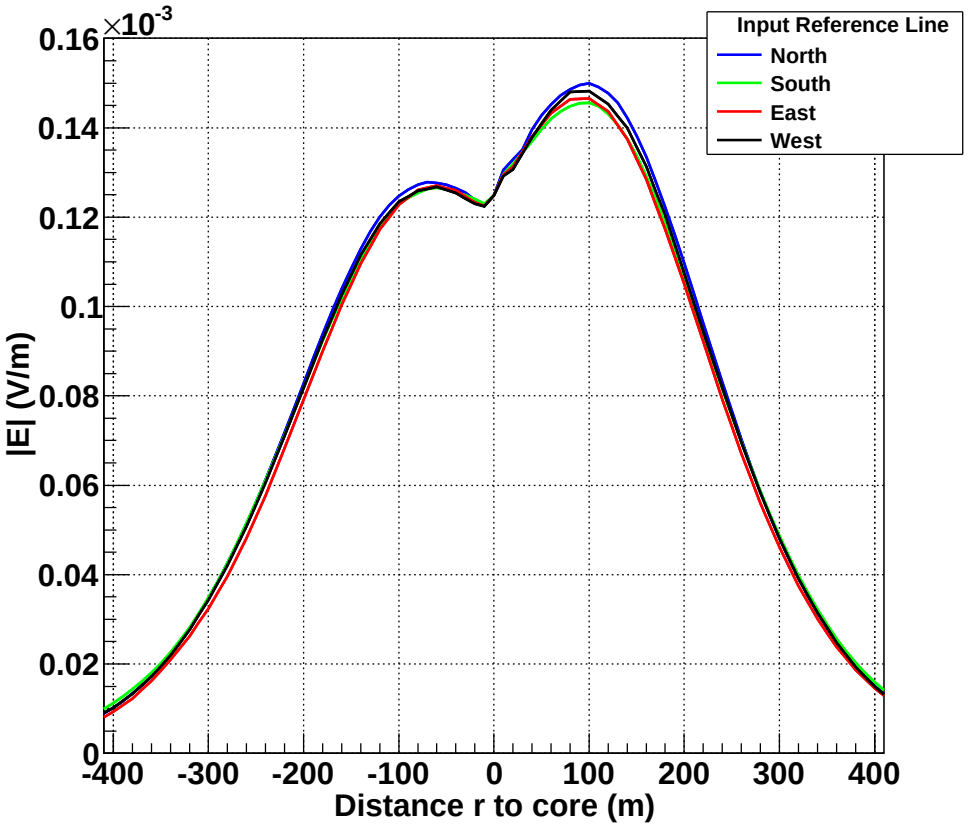

Fig. 7. Modulus of the total electric field $|\vec{E}|$ as a function of distance to core along the W-E line (for the same geometry as in Fig. 4). The electric field was obtained from the simple model using as input the electric field simulated along 4 different reference lines one at a time, namely using observer positions along the North, South, East and West directions from the shower core.

larger signals in the Northern reference line than in the Southern one. This effect is propagated to the predicted field amplitude of the model, which is 3% larger when the North direction is used as input compared to that obtained with the South line as reference, for this particular shower geometry. When the West or East directions are used as input, the fields tend to fall in between the predictions obtained using the North and South reference lines as could be expected, what is particularly clear at the Cherenkov peaks. This early/late effect diminishes near the core, where the N and S antennas have equivalent distances to points along shower axis. On the other hand the effect increases as the shower zenith angle θ rises, since differences in distance to shower from observers located N and S of the core become much more relevant.

4.3 Sources of inaccuracies

Our simple model predicts the electric field to a few percent when compared to full simulations in the vast majority of shower-observer geometries as shown in Section 4.2. However, in a few particular cases the inaccuracies in the predicted field become more apparent. The main sources of inaccuracies arise from deviations from the assumptions listed in Section 3 and the extent to which each of these deviations affects the predicted electric field depends on the geometry of the shower/observer system.

One of them is related to the input of the model and the way in which separate the Askaryan and geomagnetic contributions to the electric field amplitudes (assumption C.2. in Sec. 3.1.). These could arise because the spatial structure of the shower changes as we turn off the magnetic field in the simulation and because of small differences in the time structure of the geomagnetic and Askaryan pulses. However, since in most cases we get a very good approximation of the full simulation by using the separate contributions, these errors must be small.

We assumed a radial symmetry for the amplitude of the electric fields in the shower plane. However, when these fields are projected onto ground, there are deviations from the assumed elliptical symmetry for the amplitudes. These deviations arise from differences in the shower-observer distances between the early and late regions on the ground. These early/late effects induce only very small inaccuracies in the predicted electric field in the case of low zenith angle showers, but become larger as the zenith angle increases ($\sim 5\%$ at the peak for the 70° shower shown in the bottom panel of Fig. 6).

We have checked that the geomagnetic polarization assumed in Eq. (2) describes well that obtained in full Monte Carlo simulations at all relevant distances to the shower core. However this is not the case for the Askaryan polarization at small distances to the core and manifests into larger opening angles between the expected and fully simulated polarizations. This makes our model less accurate for the prediction of the polarization of the net electric field in vertical showers $\theta \lesssim 20^\circ$ in the case of observers near the shower core at distances $r = 0.25\ r_{\rm Cher} \sim 20$ m as can be seen in Fig. 5.

Inaccuracies also arise in the electric field amplitude predicted by the model due to the vector addition of the Askaryan and geomagnetic polarizations (Eq. 6). In fact the model is less accurate when the shower-observer geometry is such that the geomagnetic component of the emission is either smaller or has approximately the same magnitude as the Askaryan one and the observer is placed at positions on the ground where both fields point in opposite directions, even when the discrepancies between the expected and fully simulated

polarizations are small. For the geometries of the simulated showers used in this work, this occurs along the W-E line of antennas, either West or East of the core. In those geometries the model predicts a small total electric field due to the cancellation of the geomagnetic and Askaryan contributions. Several examples are shown in the right panels of Fig. 8 and represent some of the worst agreements between model and simulation of all studied showers. For instance, in the particular case of a shower coming from the North with $\theta = 60^\circ$ and observers along the West to East line at the Auger site depicted in the bottom right panel, the expected Askaryan and geomagnetic polarizations are both horizontal (parallel to the W-E line), and point in opposite directions East of the core. The geomagnetic contribution dominates the emission up to $r/r_{\rm Cher} \simeq 1$, where it is equal to the Askaryan one, while for larger distances the Askaryan mechanism is slightly dominant. In this scenario, the electric field cancels in the model at a distance $r/r_{\rm Cher} \simeq 1$ (East of the core). In contrast, this perfect cancellation does not occur in the simulation, as can be seen in the same figure. However, although the differences between the model and full simulations are quite evident, they are still small if compared to the peak value of $|\vec{E}|$ for this shower (below $\sim 5\%$). These differences may be attributed to even small deviations in the polarization in conjunction with the inherent and unknown uncertainties on the amplitude of the geomagnetic field due to assumption C.2 in Section 3.1. Other examples are shown in the top and middle right panels, where the Askaryan and geomagnetic fields point in opposite directions West of the core. As can also be seen in Fig. 8, these differences disappear elsewhere on the ground, where the Askaryan and geomagnetic polarizations do not have approximately opposite directions, such as West (East) of the core in the bottom (top and middle) right panel and along the whole S-N line of antennas depicted in the left panels. This means that these inaccuracies only affect observers on a very small area on the ground. Although this effect is present even when the discrepancies between the assumed and fully simulated polarizations are small, there are also regions near the core in which there is a large discrepancy in the Askaryan polarization. That leads to even larger errors in the electric field amplitudes in these regions, like the ones shown in the bottom panel of Fig. 5 for $\theta \lesssim 20^\circ$. In summary, these larger inaccuracies occur only if the Askaryan contribution is similar to or dominates over the geomagnetic emission, and only in regions on the ground where the two mechanisms have almost opposite polarizations.

It is important to stress that the geometries for which the differences between model and simulation are more sizeable, represent only a small fraction of the detectable showers. The reason for this is that the electric field induced in these showers typically has a small contribution from the geomagnetic emission mechanism, and as a consequence these showers are less likely to trigger an actual array of antennas. An exception is the case of almost vertical showers, which develop much closer to the antennas and can probably still be detected despite the small radio emission. However, the solid angle for detection of ver-

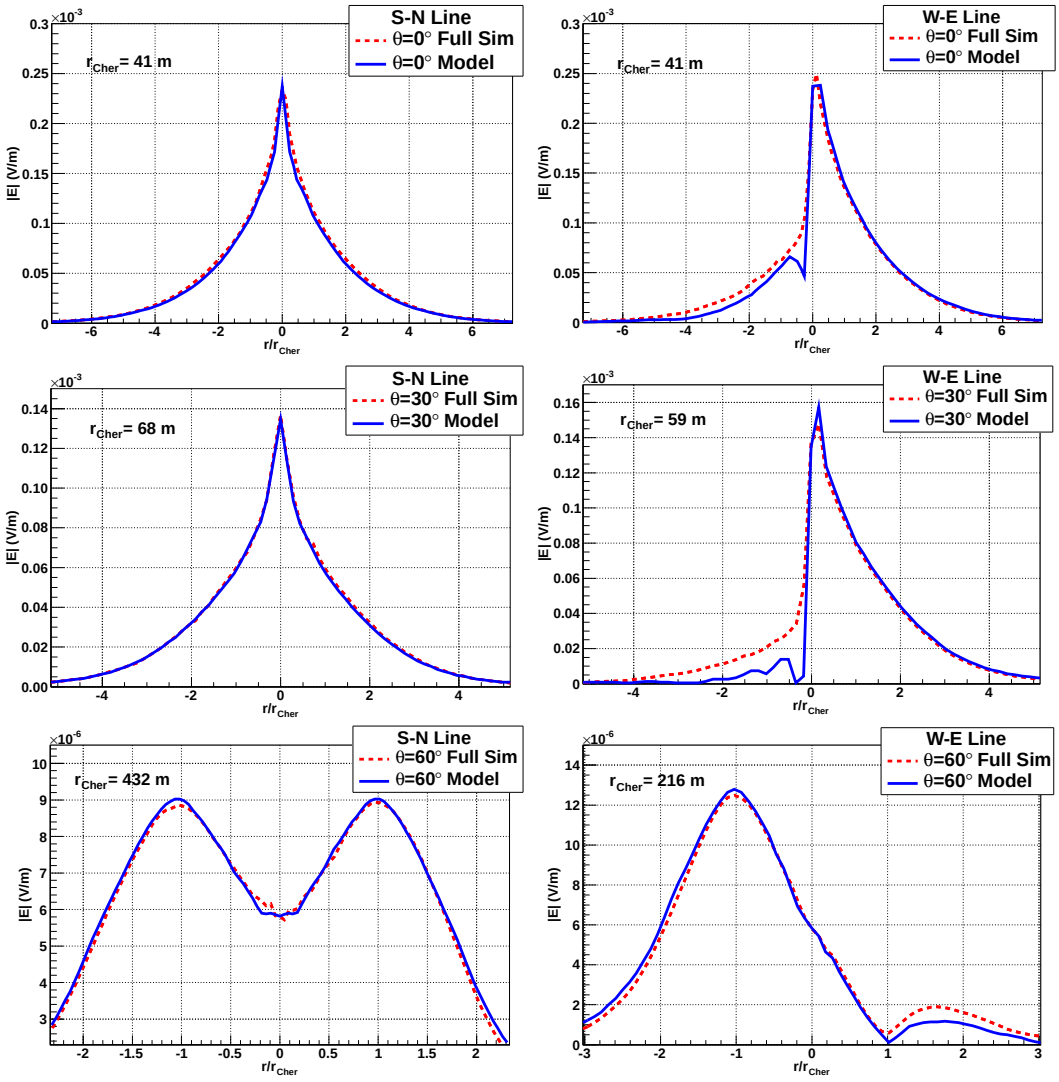

Fig. 8. Comparison of the modulus of the total electric field $|\vec{E}|$ predicted by the simple model (solid lines) with that obtained in ZHAireS simulations (dashed lines) as a function of distance to the core (normalized to the radius of the Cherenkov ring) $r/r_{\rm Cher}$ for observer positions along the West to East direction (right panels) and South to North direction (left panels) through the shower core on ground. The geometry corresponds to a proton-induced shower of energy $E = 10^{17}$ eV coming from the North at $\theta = 0°$ (top panels), $\theta = 30°$ (middle panels), and $\theta = 60°$ (bottom panels) at the Auger site. Negative values of $r/r_{\rm Cher}$ correspond to the West and South directions in the right and left panels, respectively.The value of $r_{\rm Cher}$ as obtained with Eq. (2) is also indicated in the panels.

tical showers is also very small. Furthermore, the larger differences between model and simulation tend to occur in regions where there is a strong destructive interference between both emission mechanisms, and thus even smaller net electric fields, which may be comparable to the noise floor, falling below the detection threshold of actual experiments.

5 Discussion and conclusion

We have shown that using standard assumptions on the polarization and symmetry properties of the electric field induced by the geomagnetic and Askaryan mechanisms, we are capable of estimating with great precision the electric field at any position on the ground by using as input simulations of the electric field at just a few positions. We have shown that in the majority of cases the estimates are within just a few percent of those obtained by performing time consuming full Monte Carlo simulations for all antennas. More than a simple model, this can be seen as an approach that takes into account all the complexities of the shower radio emission in a simple manner, namely by treating the two main emission mechanisms separately and looking for symmetries that do not apply to the total net electric field. Although not shown in this work, we expect our method to work at other energies and for other primaries besides the ones used here. We have also discussed the sources of inaccuracies that increase the differences between the predictions and full simulations. By refining the assumptions described in Section 3.1 to include the discrepancies found, we could not only further improve the accuracy of the model, but also better understand the main characteristics of the radio emission in the process.

The most clear advantage of using the method described in this work to predict the electric field is a significant reduction in computing time. As an illustration of what is possible we show in Fig. 3 a two-dimensional map of the electric field on the ground for which we used 36 antenna positions East of the core as input [8] . The total computing time used for the input simulations was around 10 h in a single processor. The input was used to estimate the field at antennas at every 2 m in a rectangular grid, totaling around 200 thousand antennas. This process takes just a few minutes. Our approach could also prove to be a faster alternative to radio signal interpolation techniques, which need a much larger number of simulated antenna positions on the ground to obtain similar results.

This approach may also prove to be a useful tool to simplify the creation of electric field parameterizations. As already discussed, the actual input are just two curves of $|\vec{E}|$ as a function of distance R to the core along a reference line, one for the Askaryan contribution and another for the geomagnetic one. So a parameterization of these two curves along a single arbitrary reference line as a function of the shower parameters (in a given experiment site), namely the energy E_0, shower maximum $X_{\rm max}$ and arrival direction could be used to create precise estimates of the electric field at any point on the ground. By simulating a large number of showers to create such parameterizations, one

[8] This number of antennas has not been yet optimized and can be significantly further reduced.

could obtain distributions for the parameters, making possible the inclusion of shower to shower fluctuations.

We expect the proposed method to be very useful in many applications, including the study of the characteristics of the radio lateral distribution function, such as its asymmetries and their dependence on shower parameters, and experimental reconstructions that are based on Monte Carlo simulations of the radio emission, such as the $X_{\max}$ reconstruction of the LOFAR experiment [12]. It could also be used as a test bench for new, more robust theoretical predictions for the characteristics of each emission mechanism.

6 Acknowledgments

J.A.M., W.R.C and E.Z. are supported by Ministerio de Economía (PRI-PRIMASP-2011-1154 and FPA2012-39489),the Consolider-Ingenio 2010 CPAN Programme (CSD2007-00042) and Xunta de Galicia, Consellería de Educación - Grupos de Referencia Competitivos (GRC2013-024), Feder Funds, Spain and Marie Curie-IRSES/EPLANET(European Particle physics Latin American NETwork). H.S. is supported by Office of Science, U.S. Department of Energy and N.A.S.A. We thank CESGA (Centro de Supercomputación de Galicia) for computing resources.

References

[1] T. Huege, Proceedings of the 33rd ICRC, Rio de Janeiro, Brazil (2013), available in arXiv:1310.6927 [astro-ph] (2013).

[2] M. Nagano, A. Watson, Rev. Mod. Phys. **72** (2000) 689, and references therein.

[3] F.G. Schröder for the Pierre Auger Collaboration, Proceedings of the 33rd ICRC, Rio de Janeiro, Brazil (2013), #0899.

[4] R. Gaior for the Pierre Auger Collaboration, Proceedings of the 33rd ICRC, Rio de Janeiro, Brazil (2013), #0883

[5] J. Abraham et al [Auger Collaboration], NIMA, **523** (2004) 50.

[6] D. Ardouin *et al.* [CODALEMA Collaboration], Astropart. Phys. **31** (2009) 192.

[7] A. Nigl *et al.* [LOPES Collaboration], Astron. & Astrophys. **488**, 807 (2008).

[8] D. Ardouin *et al.* [TREND Collaboration] Astropart. Phys. **34** 717 (2011) 717; O. Martineau-Huynh for the TREND Collaboration, arXiv:1204.1599 [astro-ph].

[9] P. Schellart *et al.* [LOFAR Collaboration], Astron. & Astrophys. **560** (2013) A98.

[10] F.G. Schröder for the Tunka-Rex Collaboration, Proceedings of the 33rd ICRC, Rio de Janeiro, Brazil (2013), #0452.

[11] W.D. Apel *et al.* [KASCADE & LOPES Collaborations] Phys. Rev. D **85** (2012) 071101(R).

[12] S. Buitink *et al.* [LOFAR Collaboration], Proceedings of the 33rd ICRC, Rio de Janeiro, Brazil (2013), #0579.

[13] H.R. Allan, R.W. Clay, J.K. Jones, Nature **227** (1970) 1116.

[14] W.D. Apel *et al.* [KASCADE & LOPES Collaborations] Astropart. Phys. **32** (2010) 294.

[15] S. Hoover *et al.* [ANITA Collaboration], Phys. Rev. Lett. **105** (2010) 151101.

[16] R. Smida *et al.* [CROME group], arXiv:1306.6738 [astro-ph] (2013).

[17] O. Scholten, K. Werner, F. Rusydi, Astropart. Phys. **29** (2008) 94; K. Werner, O. Scholten, Astropart. Phys. **29** (2008) 393.

[18] K. Werner, K. D. de Vries, O. Scholten, Astropart. Phys. **37** (2012) 5

[19] M. Ludwig, T. Huege, Astropart. Phys. **34**, 438 (2011).

[20] V. Marin and B. Revenu, Astropart. Phys. **35** (2012) 733.

[21] J. Alvarez-Muñiz, W.R. Carvalho, E. Zas, Astropart. Phys. **35** (2012) 325.

[22] T. Huege, C.W. James, Proceedings of the 33rd ICRC 2013, Rio de Janeiro, Brazil (2013) #548.

[23] J. Alvarez-Muñiz, W.R. Carvalho, A. Romero-Wolf, M. Tueros and E. Zas, Phys. Rev. D **86** (2012) 123007

[24] J. Alvarez-Muniz, W.R. Carvalho Jr., A. Romero-Wolf, M. Tueros and E. Zas, Proceedings of the 33rd ICRC 2013, Rio de Janeiro, Brazil (2013) #105.

[25] T. Huege, AIP Conf. Proc. **1535** (2013) 121, avaiable in 1301.2135 [astro-ph]

[26] W.D. Apel *et al.* [LOPES Collaboration] Astropart. Phys. **50-52** (2013) 76

[27] A. Aab *et al.* [Pierre Auger Collaboration] to appear in Phys. Rev. D (2014).

[28] T. Huege, R. Ulrich, R. Engel, Astropart. Phys. **30** (2008) 96.

[29] N.N. Kalmykov and A.A. Konstantinov JCAP **12** (2012) 029

[30] K.D. de Vries, A.M. van den Berg, O. Scholten, K. Werner, Astropart. Phys. **34** (2010) 267.

[31] K. D. de Vries, O. Scholten, K. Werner, Astropart. Phys. **45** (2013) 2327.

[32] H. R. Allan, in: J. G. Wilson, S. A. Wouthuysen (Eds.), Progress in Elementary Particle and Cosmic Ray Physics **10**, North Holland, (1971), p. 169, and refs. therein.

[33] J.R. Prescott, J.H. Hough, and J.K. Pidcock, Nature Phys. Science 233 (1971) 109.

[34] G.A. Askar'yan, Soviet Physics JETP **14** (1962) 441; G. A. Askaryan, Soviet Phys. JETP **21** (1965) 658.

[35] F.D. Kahn, I. Lerche, Proc. Roy. Soc. A**289** (1966) 206.

[36] J.D. Jackson, "Classical Electrodynamics" 3rd Ed. (Wiley, New York, 1998).

[37] E. Zas, F. Halzen, T. Stanev, Phys. Rev. D **45** (1992) 362.

[38] F. Halzen, E. Zas, T. Stanev, Phys. Lett. B **257** (1991) 432.

[39] D. García-Fernández, J. Alvarez-Muñiz, W.R. Carvalho Jr., A. Romero-Wolf, E. Zas, Phys. Rev. D **87** (2013) 023003.

[40] K. D. de Vries, A. M. van den Berg, O. Scholten, K. Werner Phys. Rev. Lett. **107** (2011) 061101